Supporting Information

Random Copolymerization Strategy Enables Non-Halogenated Solvent-Processed All-Polymer Solar Cells with High Efficiency over 17%

Jiabin Zhang,[a1] Qiri Huang,[a1] Kai Zhang,[a]* Tao Jia,[b]* Jianhua Jing,[a] Yuting Chen,[a] Yuhao Li,[c] Yanwei Chen,[a] Xinhui Lu,[c] Hongbin Wu,[a] Fei Huang,[a]* and Yong Cao

[a] Institute of Polymer Optoelectronic Materials and Devices, State Key Laboratory of Luminescent Materials and Devices, South China University of Technology, Guangzhou 510640, P. R. China
E-mail: mszhangk@scut.edu.cn (K. Zhang); msfhuang@scut.edu.cn (F. Huang);

[b] School of Optoelectronic Engineering, Guangdong Polytechnic Normal University, Guangzhou, 510665, China.
E-mail: tjia@gpnu.edu.cn (T. Jia);

[c] Department of Physics, The Chinese University of Hong Kong, New Territories, Hong Kong 999077, China

* Corresponding author

[1] J. Zhang. and Q. Huang contributed equally to this work.

1. Materials and synthesis

Materials.

Compound 5,8-bis(5-bromo-4-(2-butyloctyl)thiophen-2-yl)dithieno[3',2':3,4;2",3":5,6]benzo[1,2-c][1,2,5]thiadiazole (DBrDThfDTBT), polymer donor JD40 (M_n = 78.8 kDa, M_w = 176.9 kDa), PJTVT and PA-5 were synthesized according to the following literatures.[1-3] (4,8-Bis(5-(2-ethylhexyl)thiophen-2-yl)benzo[1,2-b:4,5-b']dithiophene-2,6-diyl)bis(trimethylstannane) (BDT-DSn), 1,3-bis(5-bromothiophen-2-yl)-5,7-bis(2-ethylhexyl)-4H,8H-benzo[1,2-c:4,5-c']dithiophene-4,8-dione (DBrDThBDD) was purchased from Solarmer Materials Inc. Other chemicals and solvents are purchased from Sigma, Alfa Aesar and TCI Chemical Co. and used as received.

Synthesis of JD40-BDD20:

Compound (4,8-Bis(5-(2-ethylhexyl)thiophen-2-yl)benzo[1,2-b:4,5-b']dithiophene-2,6-diyl)bis(trimethylstannane) (1) (271.3 mg, 0.3 mmol), 5,8-bis(5-bromo-4-(2-butyloctyl)thiophen-2-yl)dithieno[3',2':3,4;2",3":5,6]benzo[1,2-c][1,2,5]thiadiazole (2) (217.7 mg, 0.24 mmol), 1,3-bis(5-bromothiophen-2-yl)-5,7-bis(2-ethylhexyl)-4H,8H-benzo[1,2-c:4,5-c']dithiophene-4,8-dione (3) (46 mg, 0.06 mmol) , $Pd_2(dba)_3$ (5.4 mg) and P (o-tol)$_3$ (8.1 mg) were combined in a 48 mL sealed tube. Dry chlorobenzene (CB) (15 mL) was added under argon atmosphere. The mixture was reacted at 130 °C for 72 h. After cooled down to room temperature, the reactant mixture was poured into MeOH (200 mL). The precipitate was filtered and Soxhlet extracted with methanol, hexane, dichloromethane, and chloroform. The chloroform ingredient was concentrated, precipitated into 200 mL methanol, and dried under vacuum to afford the purple fiber JD40-BDD20 (yield 89 %, M_n = 72.9 kDa, M_w = 146.4 kDa). ^{1}H NMR (500 MHz, $CDCl_3$) δ 8.07 (s, 1.6H), 7.77 – 7.71 (m, 2.4H), 7.38 – 7.34 (m, 2H), 7.29 (m, 0.4H), 7.20 (m, 1.6H), 7.41 – 7.28 (m, 0.8H), 2.93 (m, 4H), 2.83 (m, 3.2H), 1.81 – 1.75 (m, 4H), 1.46 – 1.21 (m, 37H), 1.02 – 0.85 (m, 24H). Elemental analysis: calcd. for $C_{74.4}H_{90.8}N_{1.6}S_{8.8}$, C:68.948%, H:7.062%, N:1.729%, S:21.768%; test result, C:68.85%, H:7.046%, N:1.75%, S:21.69%.

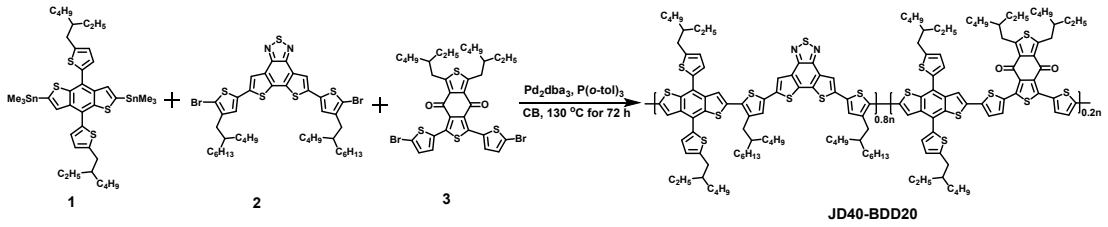

Scheme S1. The synthetic route of polymer donor JD40-BDD20.

2. Experimental Section

2.1 Characterization of photovoltaic materials

The ^{1}H NMR spectra were measured on a Bruker AV-500 MHz or Bruker AVANCE IIIT 600HD spectrometer with tetramethylsilane (TMS) as the internal reference at room temperature or 135 °C. Molecular weights of the polymers were obtained on an Acquity Advanced Polymer Chromatography (Waters) with a high-temperature chromatograph, using 1,2,4-trichlorobenzene as the eluent at 150 °C. The elemental analyses were conducted at Elementar Vario EL cube (EA) instrument. Thermogravimetric (TGA) measurements were carried out with a NETZSCH (TG209F3) apparatus at a heating rate of 10 °C min^{-1} under a nitrogen atmosphere. Differential scanning calorimetry (DSC) analysis was performed on a NETZSCH (DSC200F3) apparatus at a heating or cooling rate of 10 °C min^{-1} under a nitrogen atmosphere. Cyclic voltammetry (CV) was measured on a CHI660e Electrochemical Workstation equipped with a glassy carbon working electrode, a platinum wire counter electrode, and a saturated calomel reference electrode. The potential of saturated calomel electrodes (SCE) was internally calibrated as 0.46 V by using the ferrocene/ferrocenium redox couple (Fc/Fc^{+}), which has a known reduction potential of –4.80 eV.

2.2 Device fabrication and characterization

The conventional structure of ITO/PEDOT:PSS/Active layer/PNDIT-F3N-Br/Ag was used to fabricate all-PSCs. The indium tin oxide (ITO) substrates were cleaned sequentially by sonication with detergent, deionized water, and ethanol. After being dried in an oven at 60 °C overnight, the substrates were treated with an oxygen plasma for 4 min and then coated with PEDOT:PSS (CLEVIOS P VP Al 4083) at 3600 rpm for 30 s. After annealing at 150 °C on a hot plate in the air for 15 min, a thin film of about 40 nm was obtained. Then the substrates were transferred into an N_2

protected glove box. The corresponding all-PSCs system (Donor:acceptor=1:1.2, w/w, dissolved by *o*-XY:DMN = 99:1, *v*/*v*, with a total concentration of 12.5 mg mL^{-1}) was heated to dissolve and spin-coated with a hot solution (nearly 90 °C) onto PEDOT:PSS. And then the additive was removed from the blend film by vacuuming for two hours. Afterward, 5 nm PNDIT-F3N-Br (0.5 mg mL^{-1}) was spin-coated onto the active layers as a cathode interface. Finally, 100 nm silver was thermally deposited on top of the interface through a shadow mask in a vacuum chamber at a pressure of 1×10^{-7} mbar. The effective area of the device was confined to 0.04 cm^2 by a non-refractive mask to improve the accuracy of measurements. The current density-voltage (*J*-*V*) characteristics were measured under a computer-controlled Keithley 2400 source meter under 1 sun, AM 1.5G solar simulator (Taiwan, Enlitech SS-F5). The light intensity was calibrated by a standard silicon solar cell (certified by China General Certification Center) before the test, giving a value of 100 mW cm^{-2} during the test of *J*-*V* characteristics. The external quantum efficiency (EQE) spectra were recorded with a QE-R measurement system (Enlitech, QE-R3011, Taiwan).

2.3 Space charge limited current (SCLC) measurements

The hole-only and electron-only devices were fabricated with the architectures of ITO/PEDOT:PSS/Active layer/MoO_3/Ag and ITO/ZnO/Active layer/PFN-Br/Ag. Hole-only and electron-only devices were recorded with a Keithley 236 source meter under dark. The hole and electron mobility were determined by fitting the dark current to the model of single-carrier SCLC, which is described by the equation,

$$J = \frac{9}{8}\varepsilon_0\varepsilon_r\mu\frac{V^2}{d^3}$$

where J is the current density, μ is the zero-field mobility, ε_0 is the permittivity of free space, ε_r is the relative permittivity of the material, d is the thickness of the active layers, and V is the effective voltage. The effective voltage was obtained by subtracting the built-in voltage (V_{bi}) and the voltage drop (V_s) from the series resistance of the whole device except for the active layers from the applied voltage (V_{appl}), $V = V_{appl} - V_{bi} - V_s$. ($V_{bi} = 0$ and $V_s = 10\times I$, where the value 10 is the resistance of MoO_3 and I is the current of the devices in this work). The hole and electron mobilities can be calculated from the slope of the $J^{1/2}$-V curves.

2.4 Morphology measurements

***Transmission electron microscopy (TEM)*:** TEM images were obtained using a JEM-2100F instrument.

***Atomic force microscopy (AFM)*:** AFM measurements were carried out by using a Digital Instrumental DI Multimode Nanoscope III in a taping mode.

***Photoinduced force microscopy (PiFM)*:** The PiFM microscope is from a VistaScopefrom Molecular Vista, Inc., operated in dynamic mode using commercial gold-coated silicon cantilevers (NCHAu) from Molecular Vista. The excitation laser for the PiFM measurements is a LaserTune IR Source from Block Engineering.

***Grazing incidence small-angle X-ray scattering (GISAXS) characterization*:** GISAXS measurements were performed at beamLine 7.3.3 at the South China University of Technology. The 10 keV X-ray beam was incident at a grazing angle of 0.2^{o}. The scattered X-rays were detected using a Dectris Pilatus 2M photon-counting detector.

***Grazing incidence wide-angle X-ray scattering (GIWAXS) characterization*:** GIWAXS measurements were performed at beamLine 7.3.3 at the South China University of Technology. The 10 keV X-ray beam was incident at a grazing angle of 0.13^{o}-0.17^{o}, which maximized the scattering intensity from the samples. The scattered X-rays were detected using a Dectris Pilatus 2M photon-counting detector.

***Contact angle measurements*:** Contact angle measurements were performed using a water or diiodomethane contact angle measurement system (OCA40 Micro), and the surface energy was calculated using the equation of state.

2.5 Spectroscopic measurements

***UV-vis absorption measurement*:** UV-vis absorption spectra were recorded on a SHIMADZU UV-3600 spectrophotometer from 300 nm to 1000 nm, corrected for quartz absorption.

***Photoluminescence (PL) measurement*:** PL data were collected using the HORiBA FLUOROMAX-4 fluorimeter. The PL excitation wavelength was set to 580 nm and 750 nm.

***Transient photovoltage (TPV) measurement*:** The TPV technique using PAIOS was based on monitoring the photovoltage decay upon a small optical perturbation during different constant bias light-intensity. Variable bias light intensities lead to a range of V_{OC} to be studied. A small optical perturbation (<3% of the V_{OC}, so that $\Delta V_{OC} \ll V_{OC}$)

was applied. The subsequent voltage decay was then also recorded to directly monitor nongeminate charge carrier recombination. The photovoltage decay kinetics of all devices follows a mono-exponential decay: $\delta V = Aexp(-t/\tau)$ where t is the time, and τ is the charge carrier lifetime.

***Charge-extraction (CE) measurement*:** The CE measurement of the devices were employed using PAIOS. The devices were illuminated at different light-intensity and kept an open circuit. After the light was turned off, the voltage was set to zero or taken to short-circuit condition within a few hundred nanoseconds to extract the charges. To obtain the number of extracted charges, the current was integrated.

***Transient photocurrent (TPC) measurement*:** TPC measurement was performed with a LED light illumination and a small perturbation 500 nm laser pulse (pulse width of ~7 ns). The laser is supplied by a commercial Nd:YAG OPO (Oppolette), at a constant repetition rate of 20 Hz. The photocurrent is generated with a photovoltage signal coupled to a 50 Ω resistor, recorded by an oscilloscope (Tektronix TDS 3052C).

***EL measurement*:** The electroluminescence spectra were acquired by a high-sensitivity spectrometer (QE Pro and NIR Quest 512, Ocean Optics), while the external quantum efficiency of EL was determined by measuring the emitted photons in all directions through an integrated sphere by using a calibrated spectrometer (QE Pro, Ocean Optics), with the device injected by an external current/voltage source with constant current density.

3. Supplementary Figures and Tables

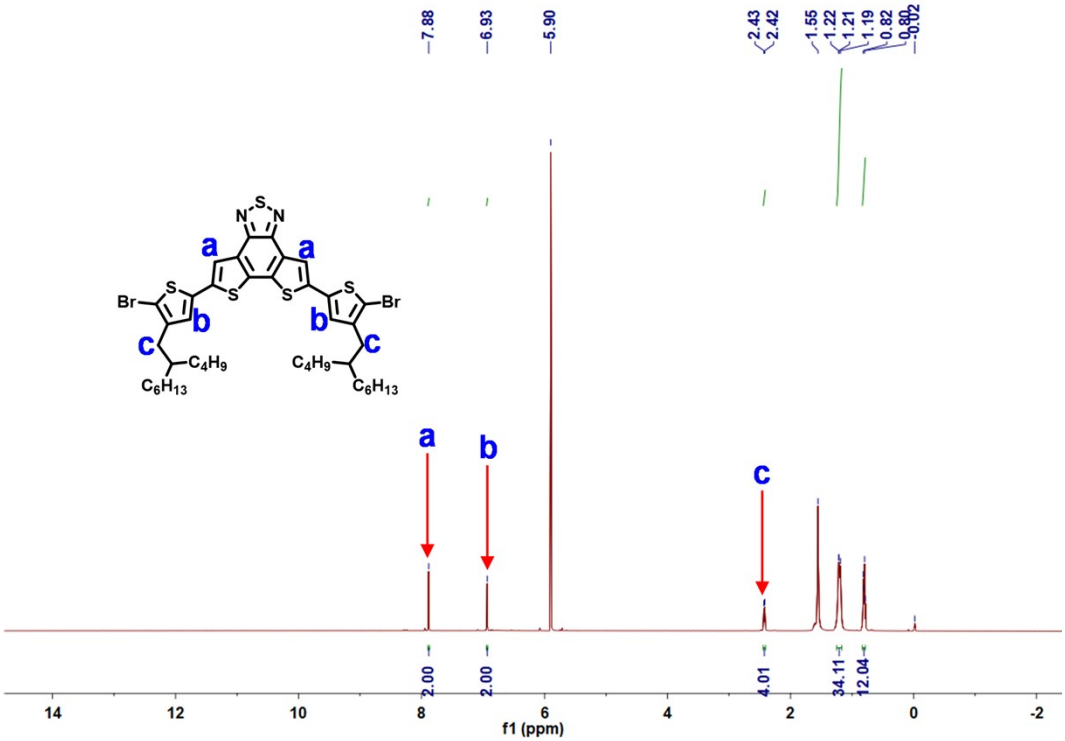

Fig. S1 The ^{1}H NMR spectrum of DBrDThfDTBT monomer in $C_2D_2Cl_4$ at room temperature.

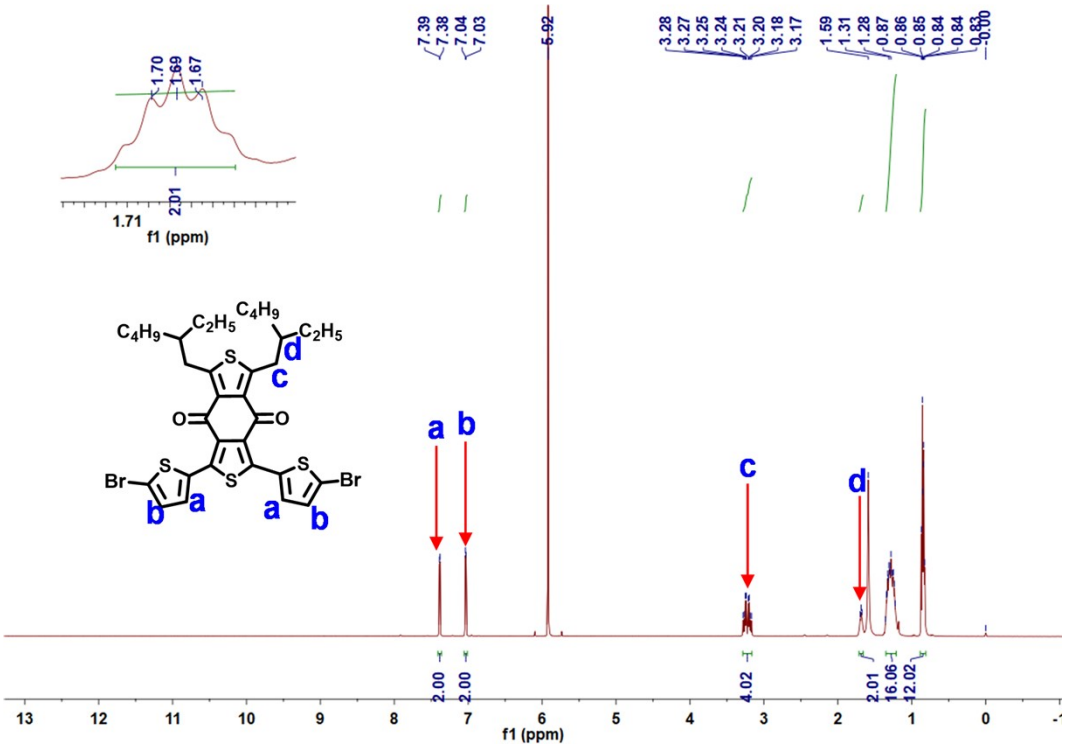

Fig. S2 The ^{1}H NMR spectrum of DBrDThBDD monomer in $C_2D_2Cl_4$ at room temperature.

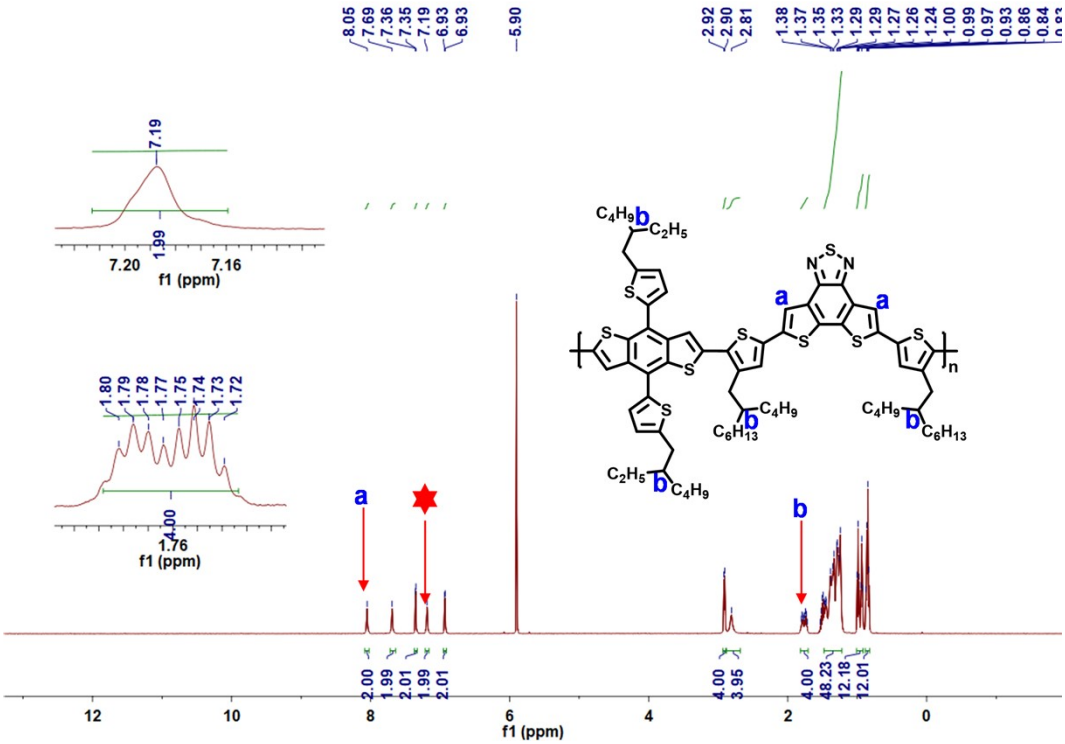

Fig. S3 The high temperature ^{1}H NMR spectrum of JD40 in $C_2D_2Cl_4$ at 135 °C.

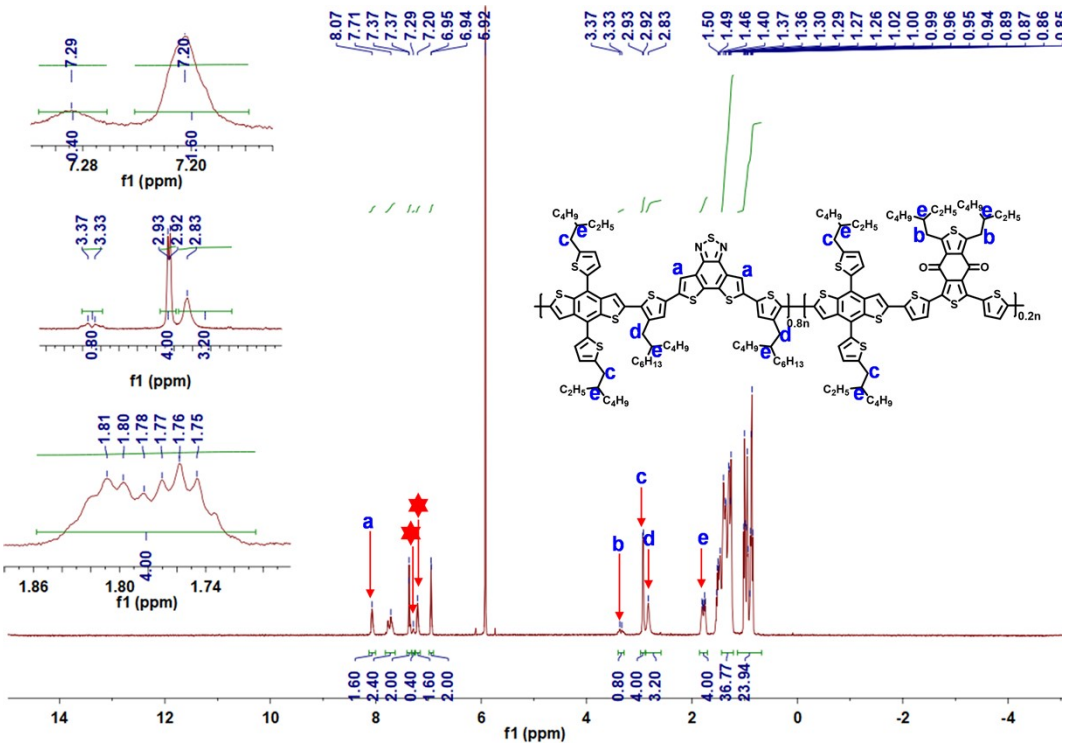

Fig. S4 The high temperature ^{1}H NMR spectrum of JD40-BDD20 in $C_2D_2Cl_4$ at 135 °C.

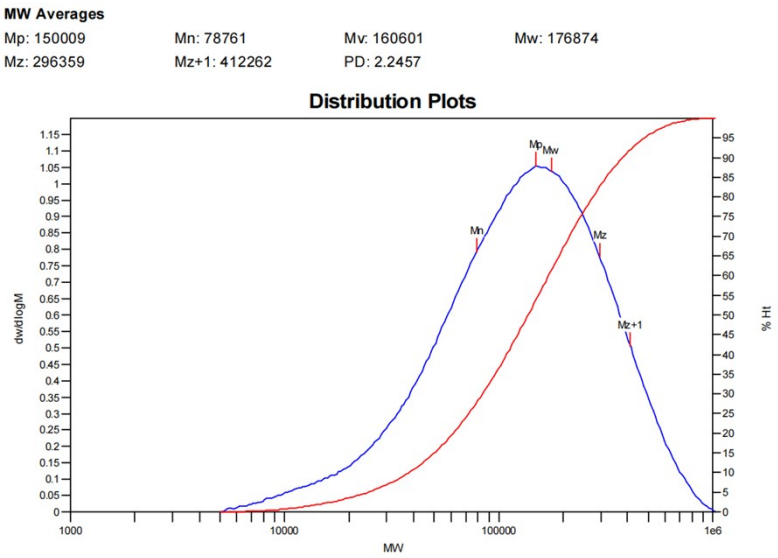

Fig. S5 High-temperature GPC measurement of JD40.

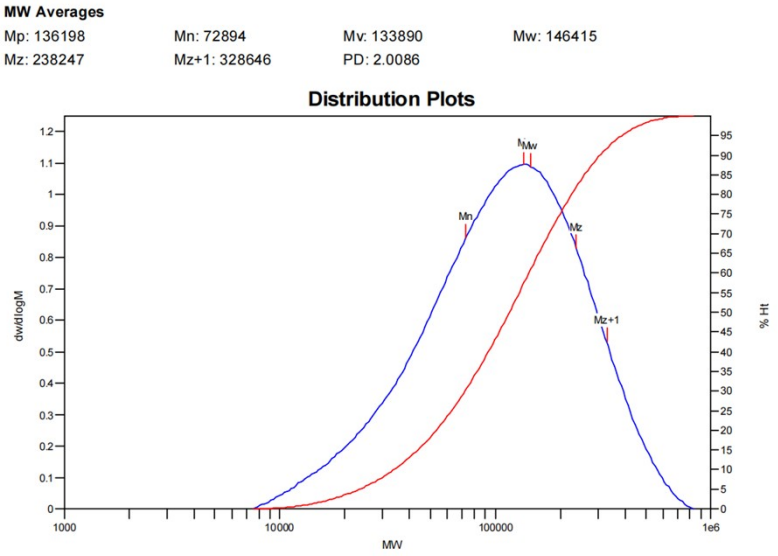

Fig. S6 High-temperature GPC measurement of JD40-BDD20.

Document:Untitled(vario EL cube) from:--.--.--(modified)

Analytic functional testing
Vario EL cube
Serial number:19103023
Text report

Weight(mg)	Name	C[%]	N[%]	H[%]	S[%]
3.7420	Sulfanilamide	41.81	16.25	4.650	18.620
2.9640	20220812-9031-A1	68.85	2.20	7.234	21.722
3.1050	20220812-9031-A1	68.80	2.19	7.201	21.754

Fig. S7 The elemental analysis result of JD40 polymer.

Document:Untitled(vario EL cube) from:--.--.--(modified)

Analytic functional testing
Vario EL cube
Serial number:19103023
Text report

Weight(mg)	Name	C[%]	N[%]	H[%]	S[%]
3.7420	Sulfanilamide	41.81	16.25	4.650	18.620
3.2010	20220812-9031-A3	68.85	1.75	7.046	21.690
2.5640	20220812-9031-A3	68.82	1.74	7.006	21.689

Fig. S8 The elemental analysis result of JD40-BDD20 polymer.

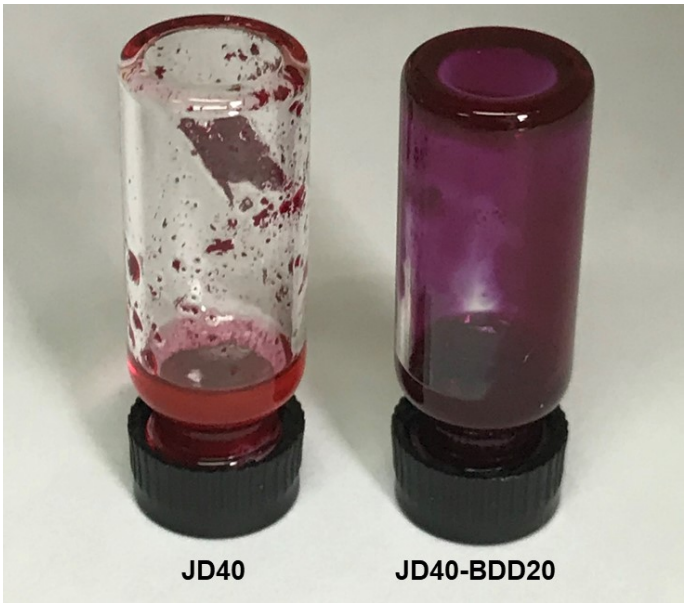

Fig. S9 The photographs of P_Ds in *o*-XY solvent with the concentration 4 mg mL^{-1} at 80 °C.

Table S1. The solubility of two donors in commonly used solvents.

Solvent	**Concentration (mg mL^{-1})**	**Temperature (℃)**	**JD40**	**JD40-BDD20**
Chloroform	4	50	⚐	⚑
		80	⚑	⚑
	6	50	⚐	⚑
		80	⚑	⚑
	8	50	⚐	⚑
		80	⚑	⚑

	10	50	⚐	⚑
		80	⚐	⚑
	15	50	⚐	⚑
Chlorobenzene	4	50	⚐	⚑
		80	⚑	⚑
	10	50	⚐	⚑
		80	⚑	⚑
	15	50	⚐	⚑
		80	⚐	⚑
o-XY	0.1	80	⚐	⚑
	4	50	⚐	⚐
		80	⚐	⚑
		100	⚐	⚑
		120	⚑	⚑
	6	80	⚐	⚑
	8	80	⚐	⚑
	10	80	⚐	⚐
		100	⚐	⚑
Methyl tetrahydrofuran	0.5	80	⚐	⚐
	2	80	⚐	⚐
CH_3OH	0.5	80	⚐	⚐

“⚐” and “⚑” stand for insoluble and soluble, respectively.

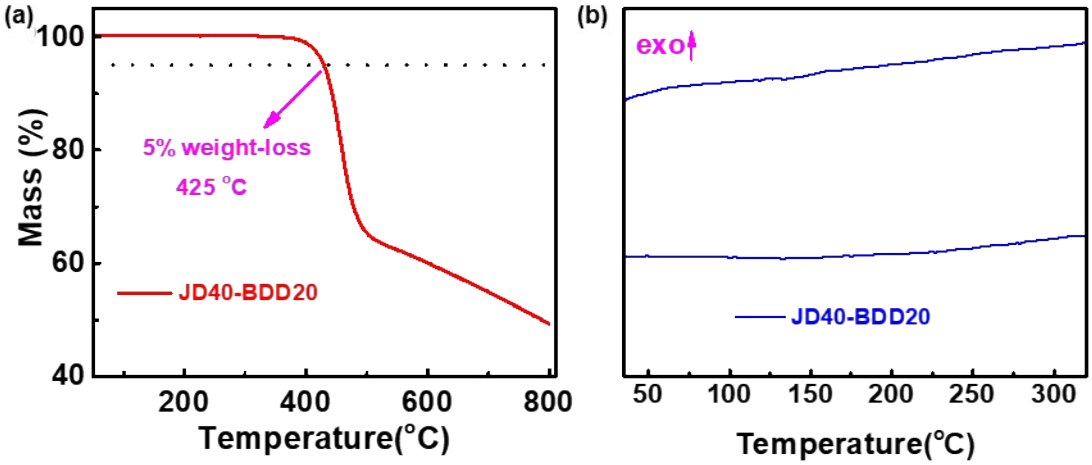

Fig. S10 Thermogravimetric analysis (a) and differential scanning calorimetry (b) curves of JD40-BDD20.

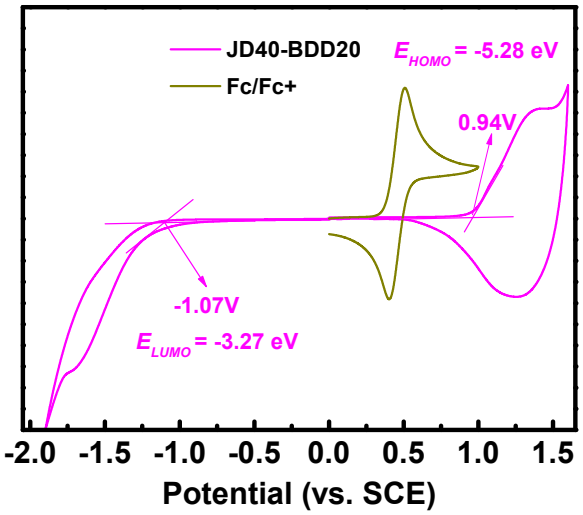

Fig. S11 Cyclic voltammetry characteristics of the JD40-BDD20.

Table S2. Molecular weights, UV–Vis absorption, electrochemical properties, and hole mobilities of JD40 and JD40-BDD20.

Donor	M_n (kDa)	M_w (kDa)	$\lambda_{sol.}^{max}$ (nm)	λ_{film}^{max} (nm)	$E_g^{opta)}$ (eV)	$E_{HOMO}{}^{b)}$ (eV)	$E_{LUMO}{}^{b)}$ (eV)	μ_h (cm^{-2} V^{-1} S^{-1})
JD40	78.8	176.9	585	586	2.12	-5.28	-3.32	3.02×10^{-3}
JD40-BDD20	72.9	146.4	580	586	2.12	-5.28	-3.27	2.31×10^{-3}

[a)] Optical bandgap estimated from the absorption onset of thin films;

[b)] Calculated from cyclic voltammetry measurement.

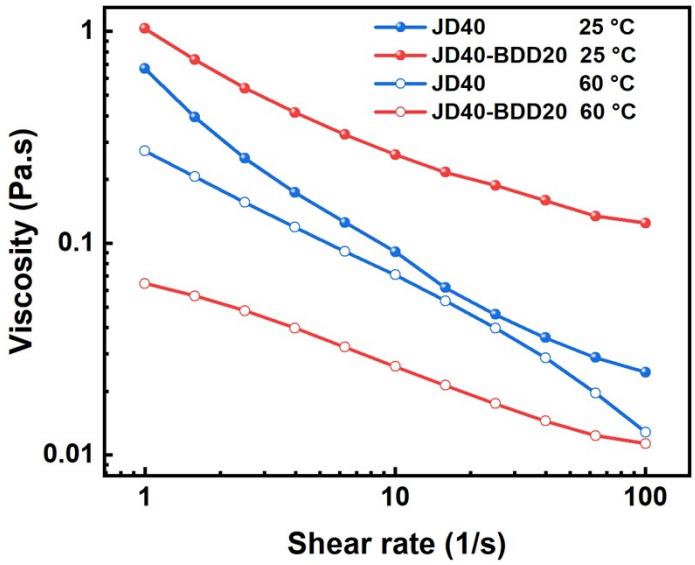

Fig. S12 Viscosity versus the shear rate of JD40 and JD40-BDD20 solution with the concentration of 4.5 mg mL^{-1} under 60 °C and 25 °C.

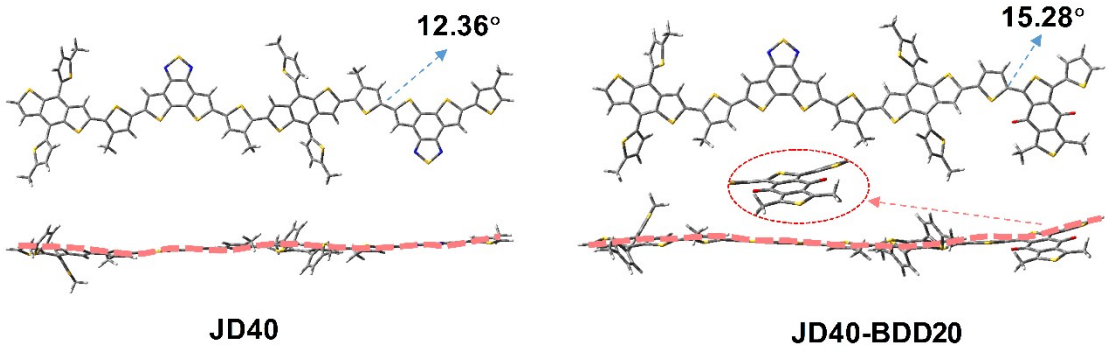

Fig. S13 The geometric structures of JD40 and JD40-BDD20 models.

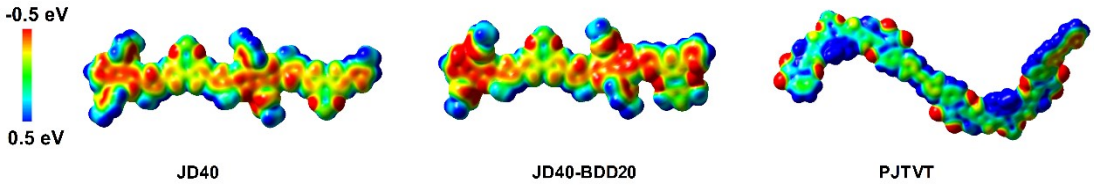

Fig. S14 The ESP distribution of JD40, JD40-BDD20, and PJTVT models.

Table S3. The ESP results of JD40, JD40-BDD20, and PJTVT models.

Material	Overall surface area	MPI	Minimal value	Maximal value	Overall average value

	(Å^2)		(Kcal/mol)	(Kcal/mol)	(Kcal/mol)
JD40	1442.82	7.18	-26.67	21.73	-0.76
JD40-BDD20	1406.01	7.58	-30.24	19.76	-1.19
PJTVT	1893.23	10.18	-36.50	37.06	3.08

Table S4**.** Photovoltaic parameters of JD40-BDD20:PJTVT all-PSCs fabricated with *o*-XY as solvent and 1% CN as an additive at the different D/A weight ratios.

D/A	V_{OC} (V)	J_{SC} (mA cm^{-2})	FF (%)	PCE (%)[a)]	PCE$_{max}$ (%)
1.5:1	0.92±0.00	20.31±0.11	67.33±2.85	12.61±0.64	13.18
1:1	0.91±0.00	22.13±0.33	72.74±1.80	14.70±0.35	15.18
1:1.2	0.91±0.00	22.30±0.22	75.68±0.46	15.41±0.13	15.64
1:1.5	0.92±0.00	16.72±0.51	70.41±2.04	10.78±0.58	11.64

[a)] The average PCE values with standard deviations were obtained from over 8 devices.

Table S5**.** Photovoltaic parameters of JD40-BDD20:PJTVT all-PSCs fabricated with *o*-XY as the solvent and 1% CN as an additive at the same D/A weight ratio (1:1.2).

Concentration	V_{OC} (V)	J_{SC} (mA cm^{-2})	FF (%)	PCE (%)[a)]	PCE$_{max}$ (%)
12 mg mL^{-1}	0.91±0.00	22.12±0.19	76.07±0.25	15.32±0.14	15.46
12.5 mg mL^{-1}	0.91±0.00	22.35±0.46	75.49±0.19	15.42±0.29	15.82
13 mg mL^{-1}	0.92±0.00	22.13±0.20	74.86±0.37	15.19±0.08	15.25

[a)] The average PCE values with standard deviations were obtained from over 8 devices.

Table S6**.** Photovoltaic parameters of JD40-BDD20:PJTVT all-PSCs fabricated with different additives and additive ratios at the same D/A weight ratio (1:1.2).

Additive	V_{OC} (V)	J_{SC} (mA cm^{-2})	FF (%)	PCE (%)[a)]	PCE$_{max}$ (%)

none	0.90±0.00	22.02±0.62	70.70±0.52	13.97±0.31	13.29
1% CN	0.91±0.00	22.35±0.46	75.49±0.19	15.54±0.29	15.82
1% DMN	0.91±0.00	23.46±0.33	74.30±1.07	15.83±0.10	16.02
1.5% DMN	0.90±0.00	21.41±0.02	72.14±1.53	13.92±0.28	14.12
2% DMN	0.90±0.00	20.23±0.27	73.23±0.60	13.30±0.20	13.44

[a] The average PCE values with standard deviations were obtained from over 12 devices.

Table S7. Photovoltaic parameters of JD40-BDD20:PJTVT all-PSCs fabricated at different annealing temperatures.

Condition	TA	V_{OC} (V)	J_{SC} (mA cm^{-2})	FF (%)	PCE (%)[a]	PCE_{max} (%)
Solvent:	none	0.91±0.00	23.76±0.35	75.04±0.55	16.14±0.13	16.35
o-XY + 1%	100℃	0.90±0.00	22.90±0.55	76.03±0.31	15.75±0.33	16.08
DMN	120℃	0.90±0.00	23.49±0.33	75.29±0.58	15.94±0.11	16.07
D/A = 1:1.2	140℃	0.89±0.00	23.27±0.35	70.96±0.99	14.65±0.42	14.89

[a] The average PCE values with standard deviations were obtained from over 12 devices.

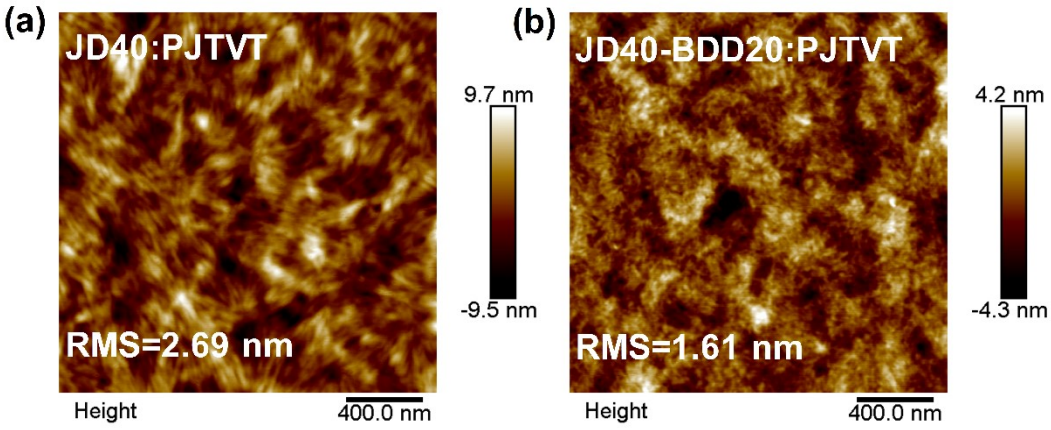

Fig. S15 AFM surface scans of (a) JD40:PJTVT and (b) JD40-BDD20:PJTVT blend film.

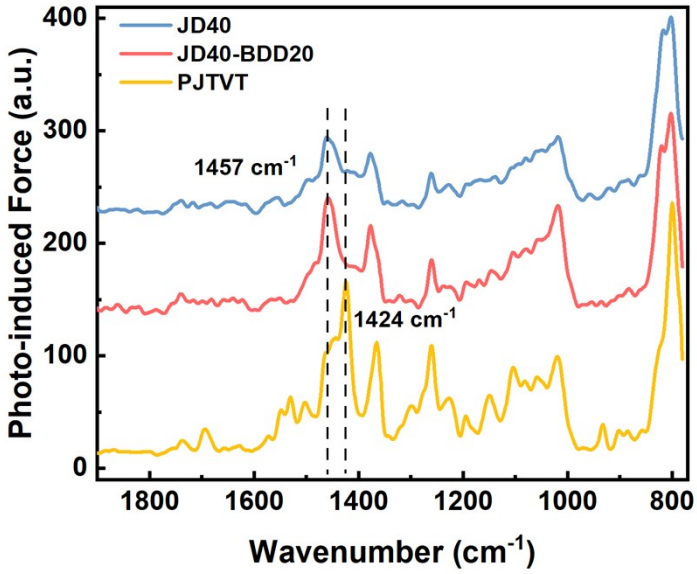

Fig. S16 The PiFM infrared (IR) spectra of pristine JD40, JD40-BDD20, and PJTVT films

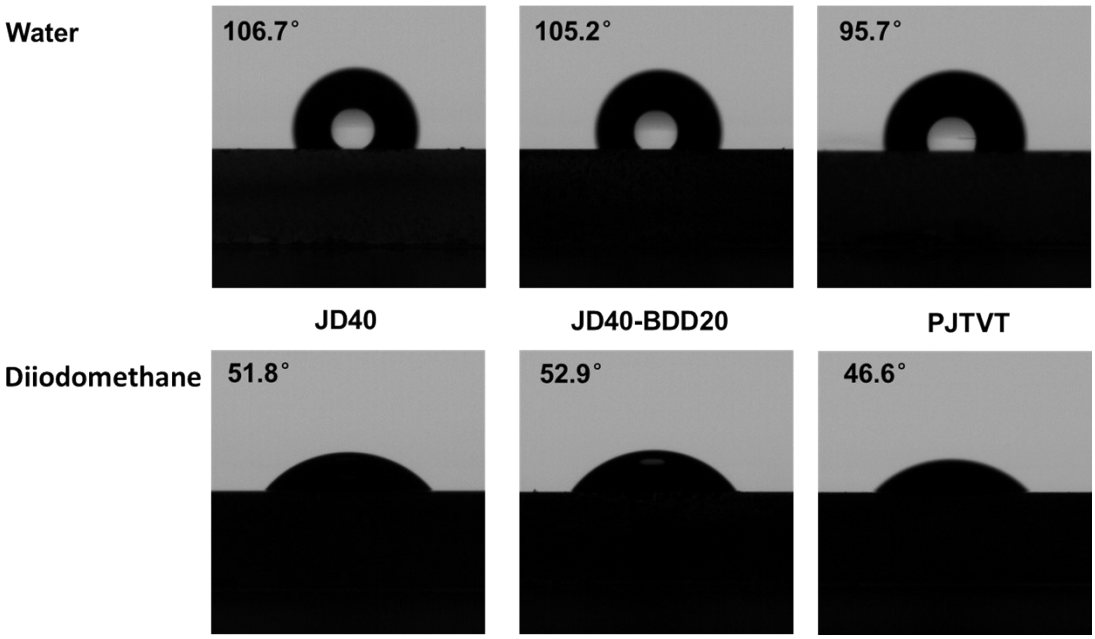

Fig. S17 Contact angle images of pristine JD40, JD40-BDD20, and PJTVT film with water and diiodomethane droplets on top.

Table S8**.** The contact angles and surface energy parameters of the polymer films.

Surface	Contact angle		γ_d[b)]	γ_p[b)]	γ	$\chi_{Donor:PJTVT}$[c)]
	θ_{water} [°]	θ_{oil} [°][a)]	[mN m^{-1}]	[mN m^{-1}]	[mN m^{-1}]	
JD40	106.7	51.8	1.34	53.72	55.06	0.304 K

JD40-BDD20	105.2	52.9	0.79	50.47	51.26	0.085 K
PJTVT	95.7	46.6	0.01	47.17	47.18	/

[a] θ_{oil} represents the contact angle of diiodomethane;

[b] γ_d and γ_p represent the surface free energies generated from the dispersion forces and the polar forces, respectively;

[c] Estimates for all Flory−Huggins interaction parameters ($\chi_{Donor:PJTVT}$) can in principle be derived using the relation of $\chi_{Donor:PJTVT} = K\,(\sqrt{\gamma_{Donor}} - \sqrt{\gamma_{PJTVT}})^2$ (K is a constant).

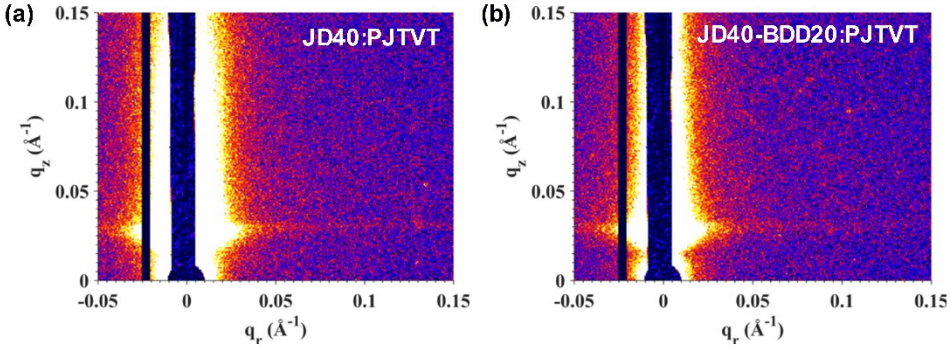

Fig. S18 2D GISAXS patterns of the (a) JD40:PJTVT blend film and (b) JD40-BDD20:PJTVT blend film.

Table S9. Morphology parameters fitted by in-plane direction intensity profiles of GISAXS (ξ is the intermixing domain size; $2R_g$ is the crystal domain size of donor).

Blend film	ξ (nm)	$2R_g$ (nm)
JD40:PJTVT	36.4	40.3
JD40-BDD20:PJTVT	35.3	25.3

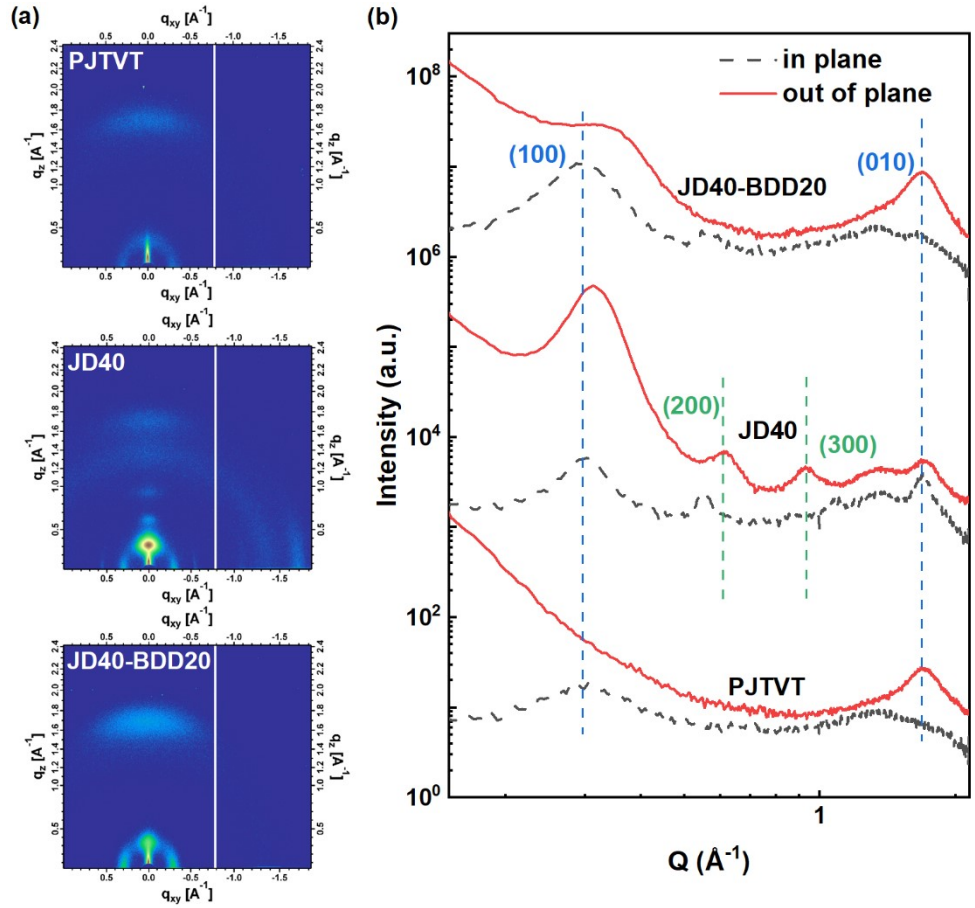

Fig. S19 (a) 2D GIWAXS patterns for the pristine films. (b) Scattering profiles of IP and OOP for pristine films.

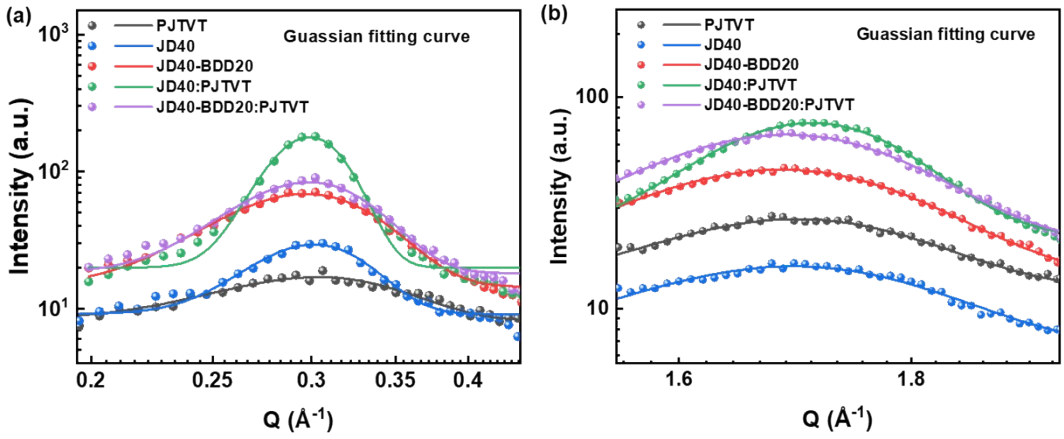

Fig. S20 The Gaussian fitting patterns of (a) (100)-IP and (b) (010)-OOP direction resulted from the GIWAXS profiles of relevant films.

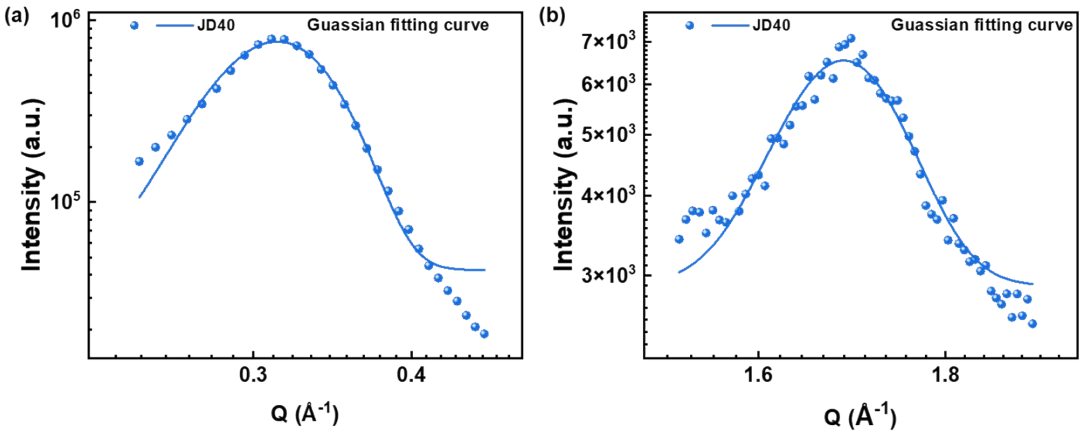

Fig. S21 The Gaussian fitting patterns of (a) (010)-IP and (b) (100)-OOP direction resulted from the GIWAXS profiles of pristine JD40 film.

Table S10. Summary of GIWAXS results in the (100)-IP and (010)-OOP.

Film	in-plane（100）				out-of-plane（010）			
	q (Å^{-1})	distance (Å)	FWHM (Å^{-1})	CCL (Å)	q (Å^{-1})	$d_{\pi-\pi}$ (Å)	FWHM (Å^{-1})	CCL (Å)
PJTVT	0.30369	20.68	0.09805	57.64	1.6989	3.70	0.22038	25.65
JD40	0.30122	20.85	0.06039	93.59	1.6956	3.70	0.24569	23.00
JD40-BDD20	0.29676	21.16	0.08001	70.64	1.68581	3.73	0.23546	24.00
JD40:PJTVT	0.29887	21.01	0.04118	137.25	1.71097	3.67	0.16845	33.55
JD40-BDD20:PJTVT	0.29851	21.04	0.07027	80.74	1.68971	3.72	0.21606	26.16

Table S11. Summary of GIWAXS results in the (010)-IP and (100)-OOP.

Film	out-of-plane（100）				in-plane（010）			
	q (Å^{-1})	distance (Å)	FWHM (Å^{-1})	CCL (Å)	q (Å^{-1})	$d_{\pi-\pi}$ (Å)	FWHM (Å^{-1})	CCL (Å)
JD40	0.31329	20.05	0.06333	89.25	1.688	3.72	0.13042	43.34

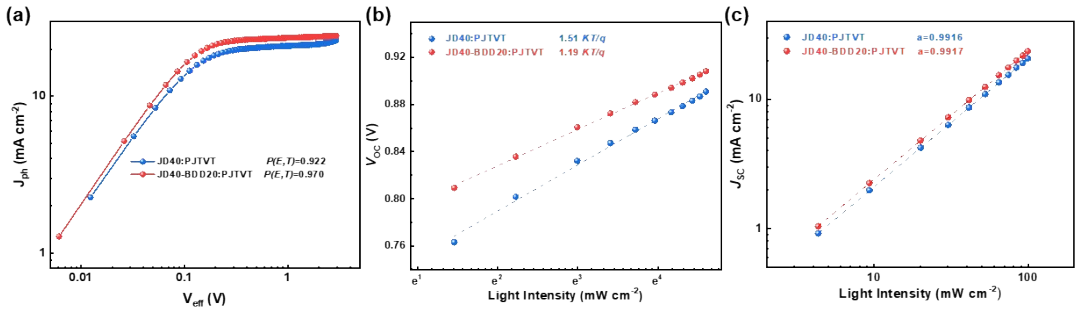

Fig. S22 (a) The exciton dissociation efficiency *P(E,T)* of the all-PSCs. (b) Measurement of V_{OC} versus light intensity of the all-PSCs. (c) Measurement of J_{SC} versus light intensity of the all-PSCs.

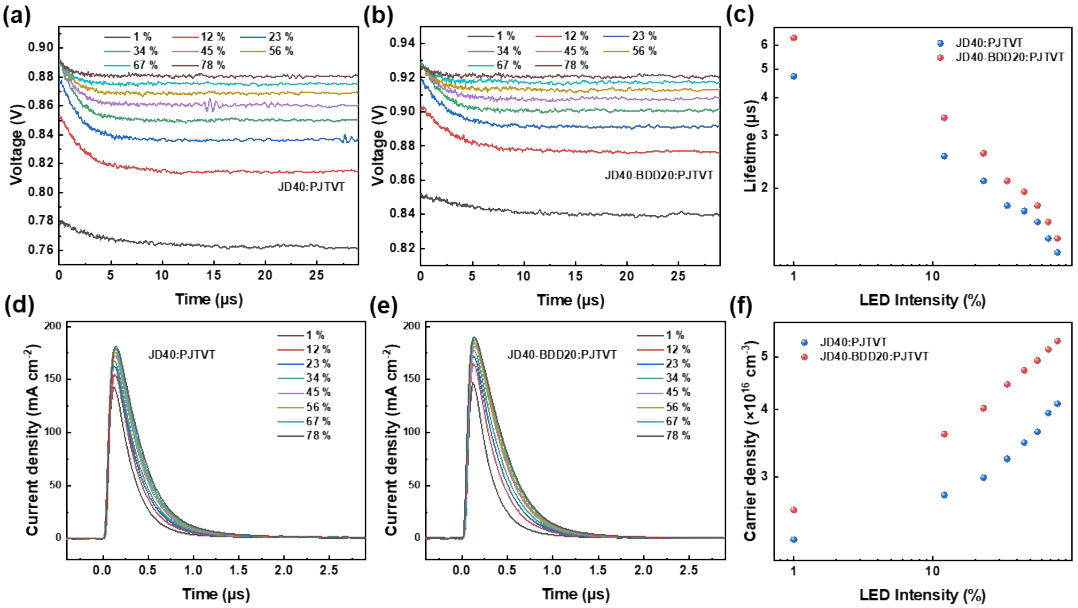

Fig. S23 Transient photovoltage traces of JD40:PJTVT (a) and JD40-BDD20:PJTVT devices (b) under different illumination intensities. (c) The carrier lifetimes under different illumination intensities. The charge extraction traces of JD40:PJTVT (d) and JD40-BDD20:PJTVT devices (e) under different illumination intensities. (f) The carrier densities under different illumination intensities.

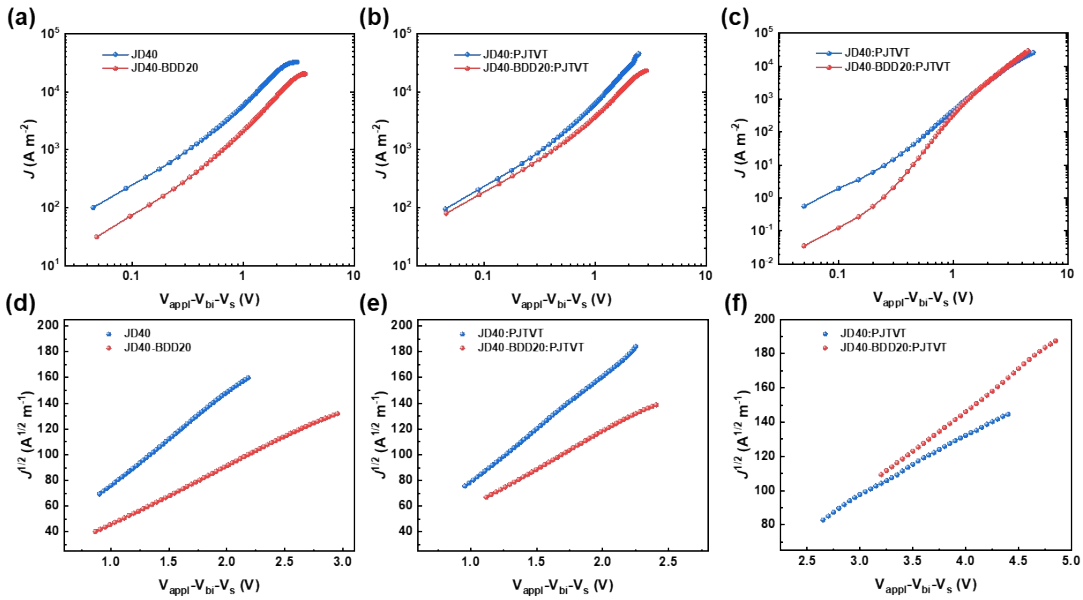

Fig. S24 Carrier mobilities. The dark *J*-*V* characteristics of (a,b) hole-only and (c) electron-only devices. The dark $J^{1/2}$–*V* characteristics of (d,e) hole-only and (f) electron-only devices.

Table S12**.** The corresponding parameters of the device were extracted from EL and FTPS-EQE spectra.

Device	E_g (eV)	$qV_{OC,SQ}$ (eV)	ΔE_1[a)] (eV)	$qV_{OC,rad}$ (eV)	ΔE_2[b)] (eV)	ΔE_3[c)] (eV)	V_{OC}^{Cal} (eV)
JD40:PJTVT	1.47	1.19	0.28	1.14	0.05	0.26	0.88
JD40-BDD20:PJTVT	1.47	1.19	0.28	1.14	0.05	0.23	0.91

[a)] The ΔE_1 depends on E_g and the theoretical maximum voltage by the Shockley–Queisser limit.

[b)] The ΔE_2 is the additional radiative recombination loss from the absorption below the band gap.

[c)] The ΔE_3 is caused by nonradiative recombination and can be calculated by $\Delta E_3 = kT\ln(EQE_{EL})$.

Table S13. Photovoltaic performances of the all-PSCs based on JD40:PA-5 and JD40-BDD20:PA-5.

Device	V_{OC} (V)	J_{SC} ($J_{SC,EQE}$) (mA cm^{-2})	FF (%)	PCE (%)[a)]	PCE_{max} (%)

JD40:PA-5	0.84	23.36 (22.34)	72.87	14.00±0.37	14.37
JD40-BDD20:PA-5	0.88	25.23 (23.99)	77.11	17.02±0.12	17.21

[a)] The average PCE values with standard deviations were obtained from over 8 devices.

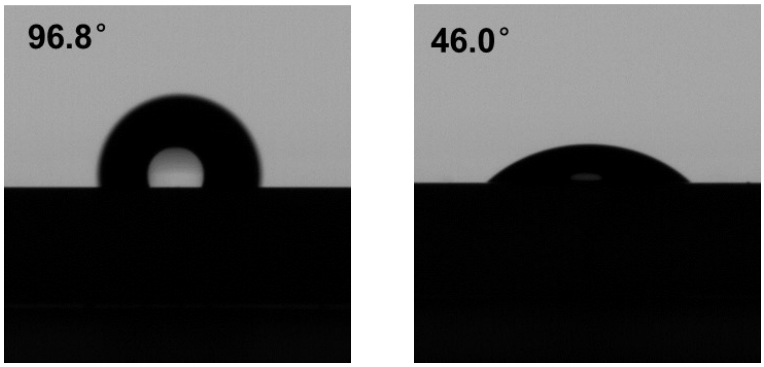

Fig. S25 Contact angle images of pristine PA-5 film with water and diiodomethane droplets on top.

Table S14**.** The contact angles and surface energy parameters of the PA-5 film.

Surface	Contact angle		γ_d	γ_p	γ	$X_{JD40:PA-5}$	$X_{JD40-BDD20:PA-5}$
	θ_{water} [°]	θ_{oil} [°]	[mN m^{-1}]	[mN m^{-1}]	[mN m^{-1}]		
PA-5	96.8	46.0	0.01	49.24	49.25	0.162 K	0.020 K

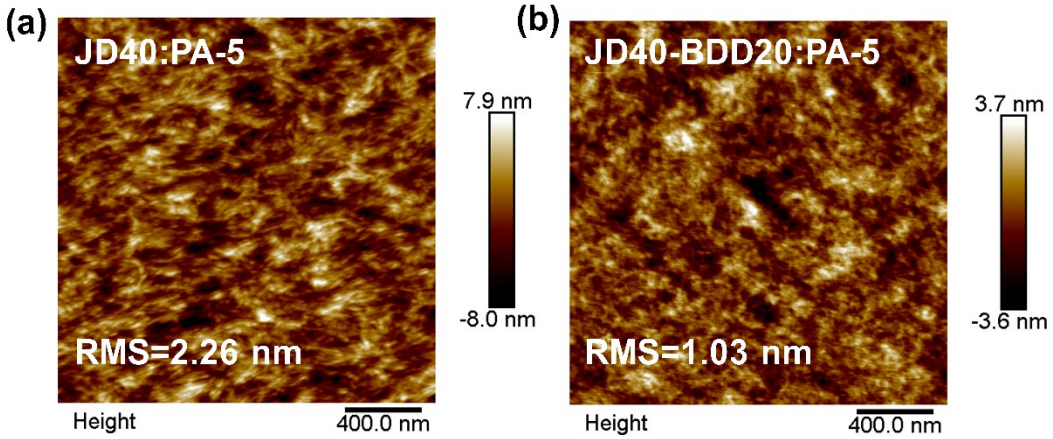

Fig. S26 AFM surface scans of (a) JD40:PA-5 and (b) JD40-BDD20:PA-5 blend film.

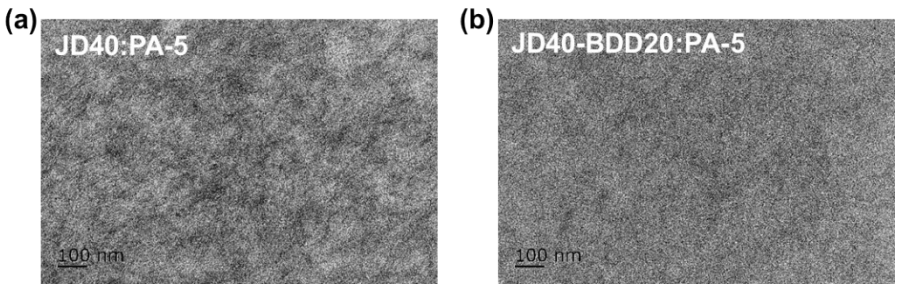

Fig. S27 TEM images of (a) JD40:PA-5 and (b) JD40-BDD20:PA-5 blend film.

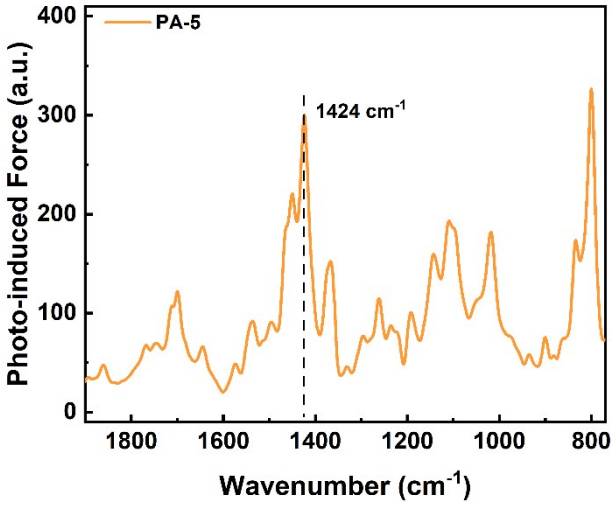

Fig. S28 The PiFM infrared (IR) spectra of pristine PA-5 film.

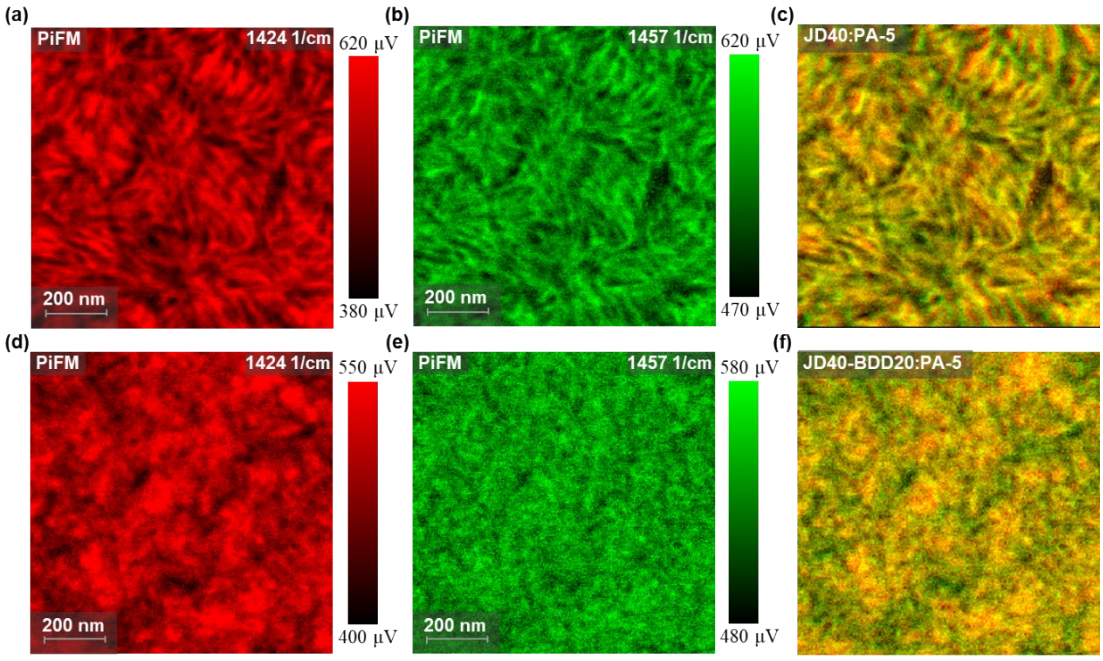

Fig. S29 PiFM images of the (a) JD40:PA-5 and (d) JD40-BDD20:PA-5 blend film at

the wavenumbers of 1424 cm^{-1} for PA-5. PiFM images of the (b) JD40:PA-5 and (e) JD40-BDD20:PA-5 blend film at the wavenumbers of 1457 cm^{-1} for the donor. (c) The combined image of (a) and (b) for the JD40:PA-5 blend film. (f) The combined image of (d) and (e) for the JD40-BDD20:PA-5 blend film.

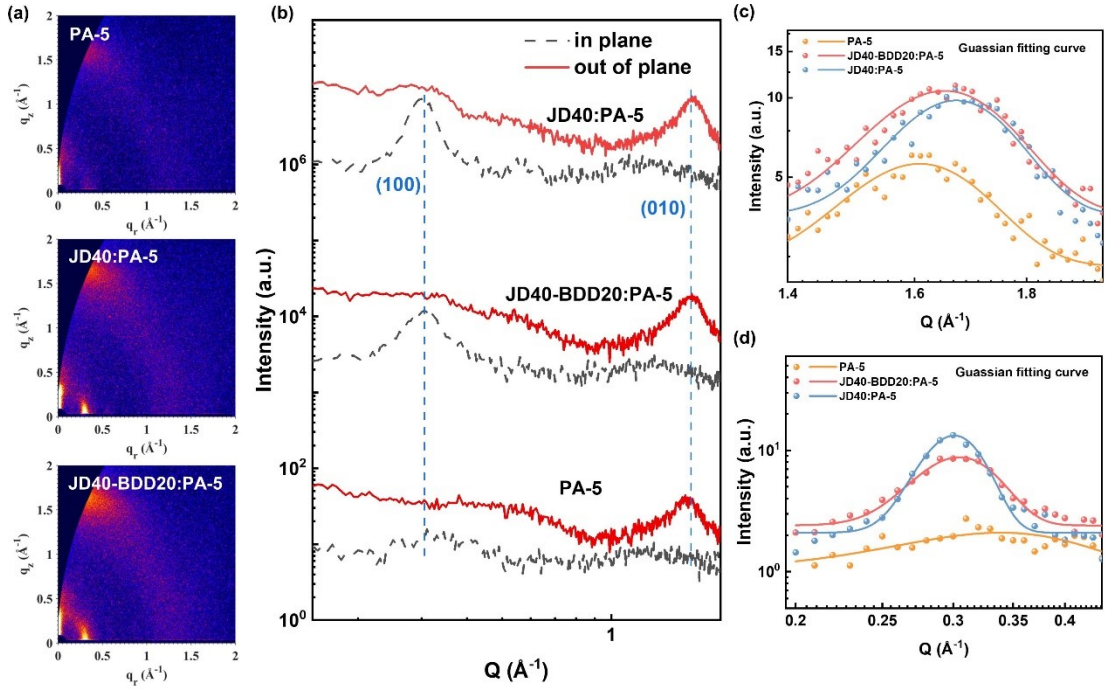

Fig. S30 (a) 2D GIWAXS patterns of the JD40:PA-5 and JD40-BDD20:PA-5 blend films. (b) Scattering profiles of IP and OOP for JD40:PA-5 and JD40-BDD20:PA-5 blend films. The Gaussian fitting patterns of (c) (010)-OOP and (d) (100)-IP direction resulted from the GIWAXS profiles of relevant films.

Table S15. Summary of GIWAXS results in the (100)-IP and (010)-OOP.

Film	in-plane（100）				out-of-plane（010）			
	q ($Å^{-1}$)	distance (Å)	FWHM ($Å^{-1}$)	CCL (Å)	q ($Å^{-1}$)	$d_{\pi-\pi}$ (Å)	FWHM ($Å^{-1}$)	CCL (Å)
PA-5	0.33933	18.51	0.15163	37.27	1.60857	3.90	0.22275	25.37
JD40:PA-5	0.30072	20.88	0.0436	129.63	1.67155	3.76	0.20086	28.14
JD40-BDD20:PA-5	0.30470	20.61	0.05873	96.24	1.65120	3.80	0.23039	24.53

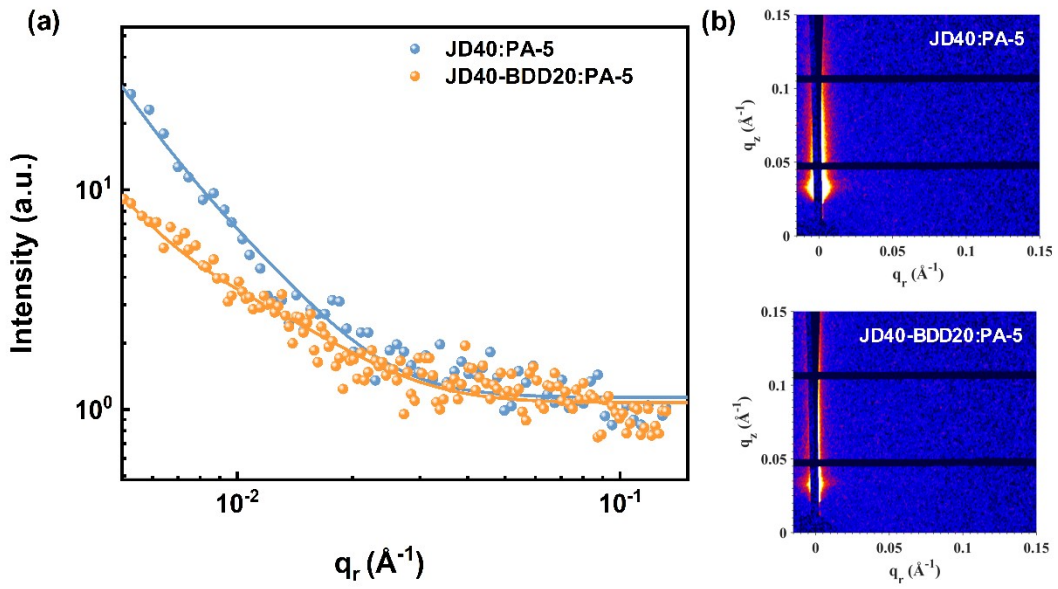

Fig. S31 (a) GISAXS intensity profiles (dotted lines) and best fittings (solid lines) along the in-plane direction of JD40:PA-5 and JD40-BDD20:PA-5 blend film. (b) 2D GISAXS patterns of the JD40:PA-5 and JD40-BDD20:PA-5 blend film.

Table S16. Morphology parameters fitted by in-plane direction intensity profiles of GISAXS (ξ is the intermixing domain size; $2R_g$ is the crystal domain size of donor).

Blend film	ξ (nm)	$2R_g$ (nm)
JD40:PA-5	37.8	37.5
JD40-BDD20:PA-5	35.2	25.9

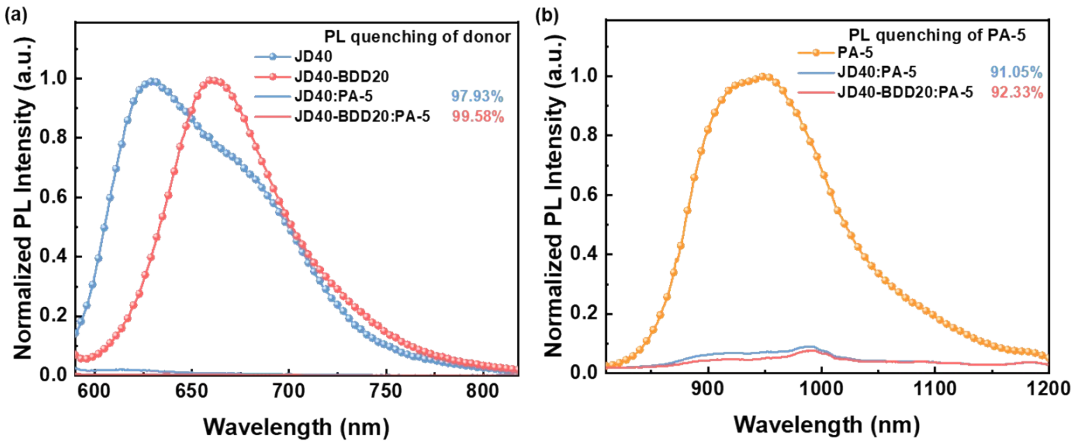

Fig. S32 (a) PL spectra of pristine donors and JD40:PA-5 and JD40-BDD20:PA-5 blend films excited at 580 nm. (b) PL spectra of pristine PA-5 and JD40:PA-5 and JD40-BDD20:PA-5 blend films excited at 750 nm.

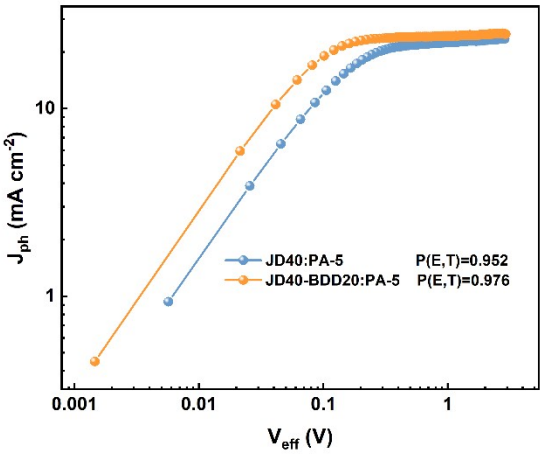

Fig. S33 The exciton dissociation efficiency *P(E,T)* of the JD40:PA-5 and JD40-BDD20:PA-5 all-PSCs.

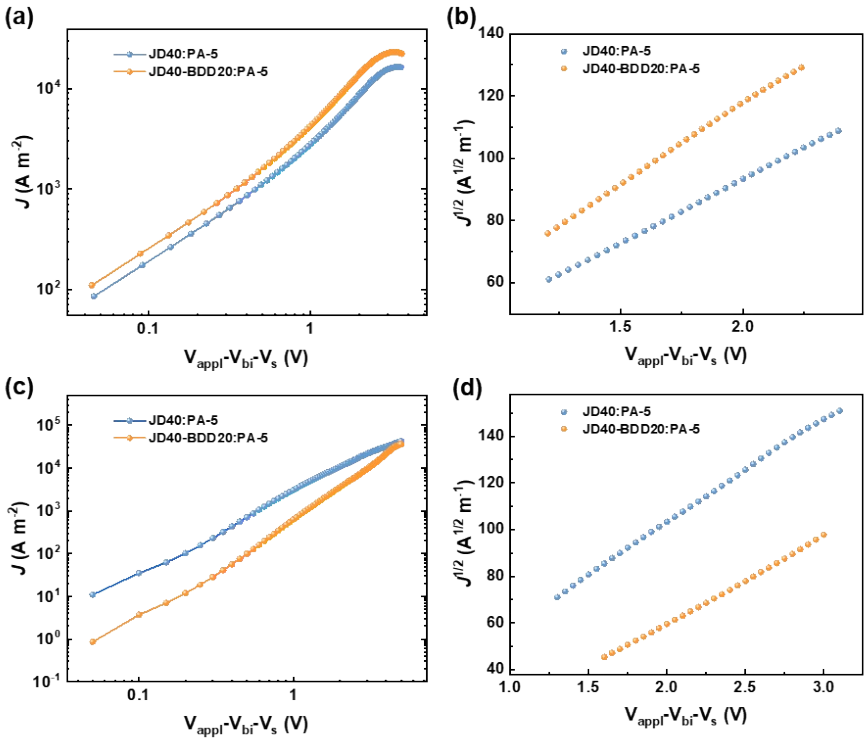

Fig. S34 Carrier mobilities. The dark *J-V* characteristics of (a) hole-only and (c) electron-only devices. The dark $J^{1/2}$–*V* characteristics of (b) hole-only and (d) electron-only devices.

Table S17. Carrier mobilities of the all-PSCs based on JD40:PA-5 and JD40-BDD20:PA-5.

Device	μ_h (cm^{-2} V^{-1} S^{-1})	μ_e (cm^{-2} V^{-1} S^{-1})	μ_h /μ_e
JD40:PA-5	1.54×10^{-3}	7.76×10^{-4}	1.98
JD40-BDD20:PA-5	9.11×10^{-4}	7.25×10^{-4}	1.26

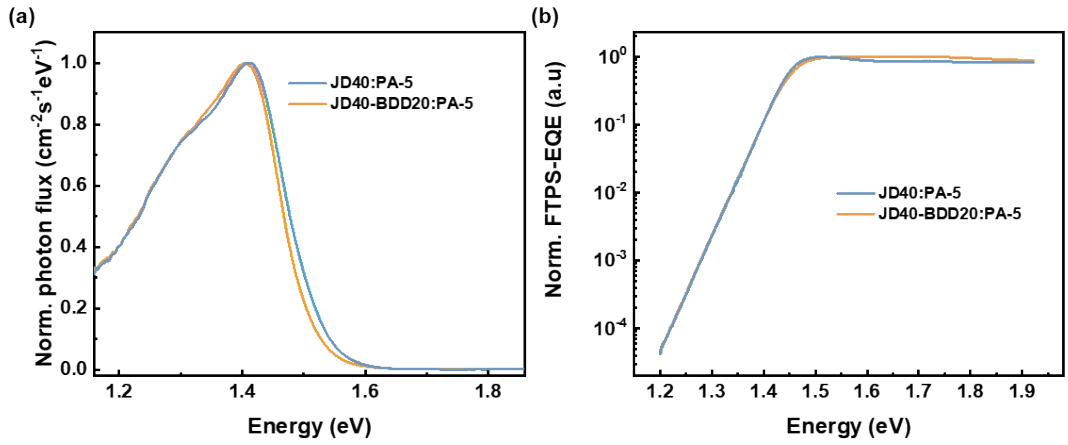

Fig. S35 (a) EL spectra of the JD40:PA-5 and JD40-BDD20:PA-5 devices. (b) FTPS-EQE spectra of the JD40:PA-5 and JD40-BDD20:PA-5 devices.

Table S18. The corresponding parameters of the device were extracted from EL and FTPS-EQE spectra.

Device	E_g (eV)	$qV_{OC,SQ}$ (eV)	ΔE_1 (eV)	$qV_{OC,rad}$ (eV)	ΔE_2 (eV)	ΔE_3 (eV)	V_{OC}^{Cal} (eV)
JD40:PA-5	1.45	1.17	0.28	1.12	0.05	0.28	0.84
JD40-BDD20:PA-5	1.45	1.18	0.27	1.12	0.06	0.24	0.88

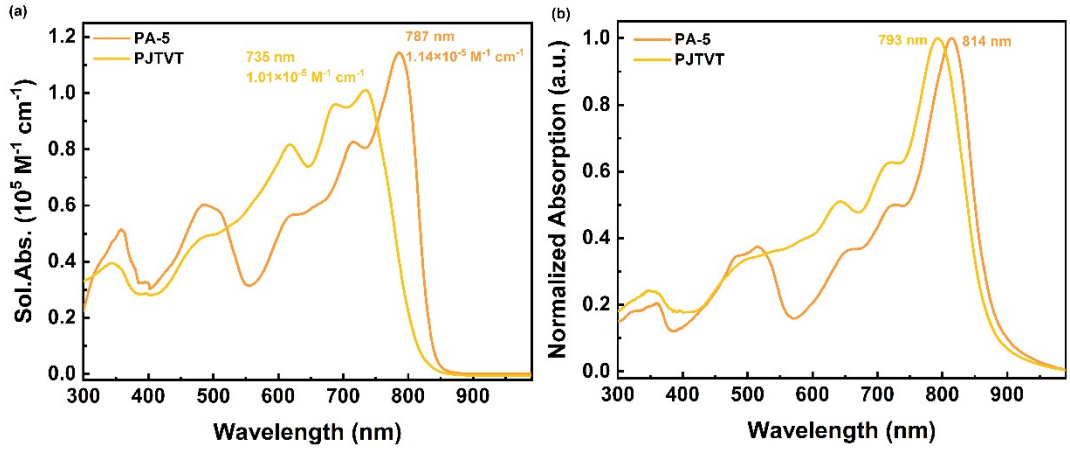

Fig. S36 UV-vis absorption spectra of PA-5 and PJTVT in (a) *o*-XY solution and (b) the corresponding pristine films.

Reference

1. T. Jia, J. Zhang, K. Zhang, H. Tang, S. Dong, C.-H. Tan, X. Wang and F. Huang, *J. Mater. Chem. A*, 2021, **9**, 8975-8983.
2 J. Zhang, C.-H. Tan, K. Zhang, T. Jia, Y. Cui, W. Deng, X. Liao, H. Wu, Q. Xu, F. Huang and Y. Cao, *Adv. Energy Mater.*, 2021, **11**, 2102559.
3 J. Jia, Q. Huang, T. Jia, K. Zhang, J. Zhang, J. Miao, F. Huang and C. Yang, *Adv. Energy Mater.*, 2022, **12**, 2103193.